Numerical study of tokamak equilibria with arbitrary flow

L. Guazzotto and R. Betti
University of Rochester and Laboratory for Laser Energetics, Rochester, New York 14623

J. Manickam and S. Kaye
Princeton Plasma Physics Laboratory, Princeton, New Jersey 08543

(Received 26 August 2003; accepted 3 November 2003)

The effects of toroidal and poloidal flows on the equilibrium of tokamak plasmas are numerically investigated using the code FLOW. The code is used to determine the changes in the profiles induced by large toroidal flows on NSTX-like equilibria [with NSTX being the National Spherical Torus Experiment, M. Ono, S.M. Kaye, Y.-K.M. Peng *et al.*, Nucl. Fusion **40**, 557 (2000)] where flows exceeding the sound speed lead to a considerable outward shift of the plasma. The code is also used to study the effects of poloidal flow when the flow velocity profile varies from subsonic to supersonic with respect to the poloidal sound speed. It is found that pressure and density profiles develop a pedestal structure characterized by radial discontinuities at the transonic surface where the poloidal velocity abruptly jumps from subsonic to supersonic values. These results confirm the conclusions of the analytic theory of R. Betti and J. P. Freidberg [Phys. Plasmas **7**, 2439 (2000)], derived for a low-β, large aspect ratio tokamak with a circular cross section. © *2004 American Institute of Physics.* [DOI: 10.1063/1.1637918]

I. INTRODUCTION

Despite the remarkable improvements in tokamak performances with respect to energy transport and macroscopic stability properties, tokamak plasmas still present formidable challenges in the so-called high-β regimes. It is intuitive that high-β regimes are very favorable for energy production by requiring relatively low magnetic fields while producing high power densities. However, high-β regimes are difficult to operate in, mostly because of macroscopic instabilities leading to the disruption of the plasma column and termination of the discharge. Another challenge for any magnetic confinement device is the one represented by the anomalous energy transport governing the energy losses through the plasma boundary, which greatly exceed the so-called classical predictions based on collisional transport theory. Whether driven by magnetic or electrostatic turbulence, anomalous transport causes a large increase in the energy losses and poses severe constraint on the amount of auxiliary power required to heat up the plasma to the high temperatures (in the 10 keV range) required for thermonuclear ignition.

In the last decade, it has been repeatedly observed in several devices (see, for example, Refs. 1–3) that when the plasma rotates either toroidally or poloidally, both the energy transport as well as the macroscopic stability improve significantly. The plasma rotation can be either spontaneous or driven by neutral beam injection or rf heating. The plasma of some recent experiments such as the National Spherical Torus Experiments (NSTX) (Ref. 4) and the Electric Tokamak (ET) (Ref. 5) are expected to rotate toroidally and poloidally, respectively, with large flow velocities comparable to the sound speed and/or the poloidal Alfvén speed. Such large velocities are likely to induce significant alterations of the equilibrium configurations because of the large dynamic forces and sub–super Alfvénic/sonic flow transitions. Indeed, a fast toroidal flow would cause a significant outward shift of the plasma density profile proportional to the square of the Alfvénic Mach number (see, e.g., Ref. 6). A more dramatic change in the equilibrium is induced by transonic poloidal flows in the range of the poloidal sound speed. Note that we define as transonic, an equilibrium with a flow velocity profile varying from subsonic to supersonic with respect to the poloidal sound speed. Indeed, it has been recently shown (see Ref. 7) that radial discontinuities develop at the transonic surface where the velocity profile varies from subsonic to supersonic. Both pressure and density profiles develop a pedestal structure with a sharp drop towards the plasma edge and a shear layer in poloidal velocity. Those sharp variations in the equilibrium profiles are not shocks but contact discontinuities where the total pressure (plasma+magnetic pressures) is continuous across the discontintuity.

Flow modified equilibria will almost certainly exhibit stability properties different from the static equilibria, which need to be investigated with new kinds of nonvariational stability codes. There have been some investigations of the effect of plasma flow and flow shear on macroscopic instabilities such as the internal (Refs. 8–11) and external[12,13] kinks, the ballooning modes (Ref. 14), and the resistive wall mode (RWM).[12,15–18] Most of this work has been carried out for the case of purely toroidal rotation except for Ref. 11 where the flow is directed poloidally. For the most part, flow shear (both toroidal and poloidal) is found to be stabilizing, while the bulk toroidal rotation can be either stabilizing or destabilizing. While the stabilizing effects of bulk toroidal rotation are due to the flow induced gyroscopic action (on the internal kink[8]) and ac wall stabilization on RWM,[12,15–18] the destabilizing effects are induced by the dynamic centrifugal force combined with the bad outboard magnetic field curvature (mostly on the external kinks[12,13]). One can specu-

late that even flow shear, in some instances, may be destabilizing as a result of the Kelvin–Helmoltz instability drive induced by the velocity gradients.[19] Therefore, one cannot reach a general conclusion on the effect of flow on plasma stability, but needs to carry out a stability analysis on a case by case basis with realistic flow velocity profiles and with the flow modified equilibria.

In this paper, we show the results of a numerical study carried out with the equilibrium code FLOW developed to study fixed boundary equilibria with arbitrary flows. FLOW solves the Grad–Shafranov–Bernoulli system of equations with a multigrid approach including finite pressure anisotropy. The code input requires the assignment of a set of free functions of the poloidal magnetic flux Ψ, which depend on the so-called closure equation governing the temperature(s) or entropy. Though, FLOW can solve the equilibrium equation with arbitrary flow, here we focus primarily on toroidally rotating equilibria with flow velocities in the range of the sound speed and poloidally rotating plasmas with velocities in the range of the poloidal sound speed. Other interesting equilibria with poloidal velocities in the range of the poloidal Alfvén speed will be presented elsewhere.

Because of the transonic discontinuities, it is clear, that the most challenging problem for an equilibrium code is to compute equilibria with transonic poloidal flows. To the best of the authors' knowledge, only two codes have been previously developed to compute compressible axisymmetric equilibria with poloidal flow. The codes CLIO (Ref. 20) and FINESSE (Ref. 21) both use a finite element approach and a Picard iteration scheme to solve the Grad–Shafranov–Bernoulli system of equations. The code CLIO was used to determine the effect of subsonic flow on the Joint European Torus (JET) (Ref. 22) equilibria and the code FINESSE was used to compute a variety of astrophysical and laboratory plasma configurations. However, it seems as none of those codes were ever used to study transonic poloidal flows and associated contact discontinuities. It is possible that those codes could be easily modified to compute transonic equilibria and resolve transonic discontinuities, most likely by minor changes to the Bernoulli equations solver. It is worth mentioning that a set of simplified equilibrium equations can be derived by assuming poloidal flow incompressible, and by introducing a vorticity function, as shown in Ref. 23 in the contest of stellarator equilibria. While relevant to large aspect ratio stellarators, incompressible equilibria are not interesting for tokamaks, where the effects of compressibility need to be retained.

The present work is organized as follows: In Sec. II, the model and general equations are described. Details on the numerical solution are contained in Sec. III, while Sec. IV illustrates the results of equilibrium calculations in the presence of purely toroidal flow and plasma anisotropy. In Sec. V, results are given for equilibria with poloidal flow and the development of discontinuous profiles.

II. GENERAL EQUATIONS

We consider an axisymmetric toroidal plasma described by the ideal magnetohydrodynamics (MHD) model. The model includes finite equilibrium flow velocity in both the toroidal and poloidal directions, finite pressure anisotropy in the parallel and perpendicular directions and an adjustable equation of state representing the standard ideal MHD closure for isentropic/isothermal flows or the kinetic closure derived from the guiding center constants of motion.

The basic MHD equations for mass and momentum conservation as well as the equilibrium Maxwell's equations can be written in the standard form

$$\nabla\cdot(\rho\mathbf{v})=0, \tag{1}$$

$$\rho\mathbf{v}\cdot\nabla\mathbf{v}=\mathbf{J}\times\mathbf{B}-\nabla\cdot\vec{\vec{P}}, \tag{2}$$

$$\nabla\cdot\mathbf{B}=0, \tag{3}$$

$$\mu_0\mathbf{J}=\nabla\times\mathbf{B}, \tag{4}$$

$$\nabla\times(\mathbf{v}\times\mathbf{B})=0, \tag{5}$$

where

$$\vec{\vec{P}}\equiv p_\perp\vec{\vec{I}}+\mu_0\Delta\mathbf{B}\mathbf{B}, \quad \Delta\equiv\frac{(p_\parallel-p_\perp)}{\mu_0 B^2} \tag{6}$$

is the plasma pressure tensor. The closure equation for the pressure depends on the collisionality regime. Highly collisional plasmas with the ion collision frequency greatly exceeding the ion cyclotron frequency are typically described by an isotropic pressure ($p_\parallel=p_\perp=p$) obeying the standard steady state form of the ideal MHD adiabatic equation

$$\mathbf{v}\cdot\nabla\frac{p}{\rho^{5/3}}=0. \tag{7}$$

Instead, collisionless plasmas exhibit large thermal equilibration of the temperature along the field lines leading to the condition

$$\mathbf{B}\cdot\nabla T=0, \tag{8}$$

where T is the plasma temperature, and p and T are related through the ideal gas equation of state $p=\rho T/A$, where $A\equiv m_i/(1+Z)$. Equations (7) and (8) represent the so-called MHD closure and can be easily solved once the flow velocity and magnetic field are determined.

Different closure equations need to be used in anisotropic collisionless plasmas. In this case, the parallel ($T_\parallel$) and perpendicular ($T_\perp$) temperatures are not equilibrated and two closure equations are needed. In this paper, the anisotropic equilibria are only considered in combination with purely toroidal flow, without a poloidal component in the velocity. For a toroidally rotating plasma with a Maxwellian distribution function depending on the guiding center constants of motion, the parallel temperature is uniform along the flux surfaces, and the perpendicular and parallel temperatures are related as indicated below:[6]

$$T_\parallel=T_\parallel(\Psi), \quad T_\perp\approx T_\parallel(\Psi)\frac{B}{B-\Theta(\Psi)T_\parallel(\Psi)}, \tag{9}$$

where $B=|\mathbf{B}|$ and, $T_\parallel(\Psi)$ and $\Theta(\Psi)$ are free functions of the poloidal magnetic flux Ψ, which is an approximate constant

of motion. The parallel and perpendicular pressures are related to the corresponding temperatures through the standard relation

$$p_{\parallel}=nT_{\parallel}(\Psi), \quad p_{\perp}=nT_{\perp}, \tag{10}$$

where n is the particle density. Equations (9) and (10) represent the so-called kinetic closure appropriate for high temperature anisotropic plasmas.

We use the standard set of cylindrical coordinates (R,φ,z), where R is the major radius of the torus, φ the toroidal angle, and z the height above the midplane. Under the assumption of axisymmetry, the magnetic field can be decomposed in a toroidal and a divergence free poloidal component $\mathbf{B}=B_{\varphi}\hat{e}_{\varphi}+\mathbf{B}_p$. The latter is expressed in terms of the poloidal flux gradient according to the well-known relation

$$\mathbf{B}_p=\frac{\nabla\Psi\times\hat{e}_{\varphi}}{R}, \tag{11}$$

where Ψ is the poloidal flux. A simple manipulation of Faraday's law [Eq. (5)] yields the following relation for the equilibrium flow in terms of a parallel and a toroidal component:

$$\mathbf{v}=\frac{\Phi(\Psi)}{\sqrt{\mu_0}\rho}\mathbf{B}+R\Omega(\Psi)\hat{e}_{\varphi}. \tag{12}$$

Here $\Phi(\Psi)$ and $\Omega(\Psi)$ are two free functions of Ψ describing the parallel and toroidal component of the velocity respectively. Observe that Eq. (12) indicates that the poloidal component of the flow depends exclusively on $\Phi(\Psi)$ while the toroidal component is a function of both Φ and Ω:

$$v_p=\frac{\Phi(\Psi)}{\sqrt{\mu_0}\rho}\mathbf{B}_p, \quad v_{\varphi}=\frac{\Phi(\Psi)}{\sqrt{\mu_0}\rho}B_{\varphi}+R\Omega(\Psi). \tag{13}$$

It is interesting to observe that a toroidal plasma cannot sustain a purely poloidal flow, since the exchange of momentum between the plasma and the magnetic field leads to a finite toroidal velocity as well. Even though, one could choose the free functions Φ and Ω in order to minimize the toroidal component of the flow, it is not possible to construct them in such a way to render the toroidal flow exactly zero. The flow velocity components in Eq. (13) can be used to solve the MHD closure equations (7) and (8), leading to

$$p=S(\Psi)\rho^{\gamma}, \tag{14}$$

where $S(\Psi)$ is a free function of Ψ, representing the plasma adiabat for $\gamma=5/3$ and the plasma temperature for $\gamma=1$.

Taking the $\hat{e}_{\varphi}$ component of the momentum equation and using the axisymmetric properties of the equilibrium leads to the following expression[6] for the toroidal field:

$$B_{\varphi}R=\frac{F(\Psi)-\sqrt{\mu_0}R^2\Phi(\Psi)\Omega(\Psi)}{1-\Phi^2(\Psi)/\rho-\Delta}, \tag{15}$$

where $F(\Psi)$ is a free function of Ψ. Equation (15) reduces to the standard form $B_{\varphi}R=F(\Psi)$ in the absence of poloidal flow ($\Phi(\Psi)=0$) and anisotropy ($\Delta=0$). The next step is to take the **B** component of the momentum equation, which after a straightforward calculation yields the well known Bernoulli equation

$$\frac{1}{2\mu_0}\left[\frac{\Phi(\Psi)B}{\rho}\right]^2-\frac{1}{2}[R\Omega(\Psi)]^2+W=H(\Psi), \tag{16}$$

where $H(\Psi)$ is a free function of Ψ and $W=W(\rho,B,\Psi)$ is the enthalpy function,[6] which depends on closure equations relating pressure, density, and temperature. Depending on the choice of the closure [Eqs. (7) and (8) for the MHD closure and Eqs. (9) and (10) for the kinetic closure], one can derive the following expressions for W:

$$W_{\mathrm{MHD}}=\frac{\gamma}{\gamma-1}S(\Psi)\rho^{\gamma-1}, \tag{17}$$

$$W_K=T_{\parallel}(\Psi)\ln\left[\frac{\rho|B-\Theta(\Psi)T_{\parallel}(\Psi)|}{D(\Psi)B}\right], \tag{18}$$

where $D(\Psi)$ is a free function characterizing the plasma density as defined later in Eq. (21).

It is important to observe that W depends on Ψ through free functions like $S(\Psi)$ for the MHD model and $\Theta(\Psi)$ for the kinetic model. It follows that even though W is in general a function of ρ, Ψ, and B [$W=W(\rho,\Psi,B)$], its Ψ dependence can be arbitrary. It is worth mentioning that the kinetic form of the enthalpy (18) is only correct for equilibria without poloidal flow, while the MHD form (17) is applicable to equilibria with arbitrary flow patterns.

The next step is to take the $\nabla\Psi$ components of the momentum equation (2) in order to derive the Grad–Shafranov equation for the poloidal magnetic flux. Adopting the MHD closure (14), one can rewrite the G–S equation that after a lengthy algebraic manipulation can be cast in the following convenient form:[24]

$$\begin{aligned}\nabla\cdot\left[(1-M_{Ap}^2)\left(\frac{\nabla\Psi}{R^2}\right)\right]=&-\frac{B_{\varphi}}{R}\frac{dF(\Psi)}{d\Psi}-\frac{\mathbf{v}\cdot\mathbf{B}}{\sqrt{\mu_0}}\frac{d\Phi(\Psi)}{d\Psi}\\&-R\rho v_{\varphi}\frac{d\Omega(\Psi)}{d\Psi}-\rho\frac{dH(\Psi)}{d\Psi}\\&+\frac{\rho^{\gamma}}{\gamma-1}\frac{dS}{d\Psi},\end{aligned} \tag{19a}$$

where the right-hand side is a linear combination of all the free functions, and $M_{Ap}^2\equiv\Phi^2(\Psi)/\rho$ represents the poloidal Alfvénic Mach number. Similarly, one can include the effect of finite anisotropy by adopting the kinetic closure Eqs. (9), (10), and (18). Since the kinetic closure is derived in the absence of poloidal flow, we set $\Phi(\Psi)=0$ and rewrite the G–S equation in the following form:[6]

$$\begin{aligned}\nabla\cdot\left[(1-\Delta)\left(\frac{\nabla\Psi}{R^2}\right)\right]=&-\rho\frac{dT_{\parallel}(\Psi)}{d\Psi}-\frac{B_{\varphi}}{R}\frac{dF(\Psi)}{d\Psi}\\&-R\rho v_{\varphi}\frac{d\Omega(\Psi)}{d\Psi}-\rho\frac{dH(\Psi)}{d\Psi}\\&+\rho\frac{\partial W_K}{\partial\Psi},\end{aligned} \tag{19b}$$

TABLE I. Physical meaning of the "intuitive" free functions.

Function	Physical meaning
$D(\psi)$	Density
$P(\psi)$	Isotropic pressure
$P_{\parallel}(\psi)$	Parallel pressure
$P_{\perp}(\psi)$	Perpendicular pressure
$B_0(\psi)$	Toroidal component of the magnetic field
$M_{\varphi}(\psi)$	Toroidal sonic Mach number
$M_{\theta}(\psi)$	Poloidal sonic Mach number

where the partial derivative of W_K with respect to Ψ has been taken at constant ρ and B. Observe that the equilibrium model has been reduced to a system of three equations, a PDE (19) and two algebraic equations (15), (16). This system can be solved numerically once the free functions

$$F(\Psi), \quad H(\Psi), \quad T_{\parallel}(\Psi), \quad \Theta(\Psi), \quad \Omega(\Psi), \quad \Phi(\Psi) \tag{20}$$

have been assigned.

Although the implementation of the problem in a numerical solver is at this point relatively straightforward, the definitions of the free functions are so far not intuitive. Equilibria are typically defined by assigning pressures, densities, velocities, Mach numbers, currents, safety factors or toroidal fields profiles instead of $H(\Psi)$, $\Theta(\Psi)$, $\Phi(\Psi)$, etc. However, one needs to recognize that in the presence of flow and/or anisotropy, the pressures, densities and velocities are not free functions and cannot be readily assigned. Following Ref. 7, we combine the functions (20) in order to generate a new set of free functions that are associated with the desired variables. The association is based on the principle that in the limit of vanishing flow and infinite aspect ratio, the (new) free functions exactly reproduce the desired variables. The advantage of this approach is in the fact that the free functions of Ref. 7 represent quasiphysical quantities that are commonly used to describe standard equilibrium configurations. In the following, this set of free functions will be assigned as input instead of the ones in (20).

In order to include anisotropic pressure, one more free function with respect to the ones defined in Ref. 7 will be needed. In particular, quasipressure will be replaced by two quasipressures, a parallel and a perpendicular one. The complete list of free functions used as input to the code, and their physical meaning is contained in Table I. The relation of the new free functions to those in (20) is shown in Table II. For the kinetic closure the analysis has been restricted to the case with purely toroidal flow.

III. NUMERICAL SOLUTION

The code FLOW uses a multigrid approach for solving the equilibrium equations. The algorithm can be summarized as follows:

(1) The Bernoulli equation (16) is solved for ρ.
(2) The Grad–Shafranov equation (19) is solved for Ψ.
(3) If the system is anisotropic, Eq. (15) is solved for the toroidal component of the magnetic field B_{φ}.

TABLE II. Relation between the two sets of free functions. R_0 is the position of the geometric axis of the plasma.

Function	Definition
$F(\Psi)$	$R_0 B_0(\Psi)$
$\Phi(\Psi)$	$\sqrt{\gamma P(\Psi) D(\Psi)}\dfrac{M_{\theta}(\Psi)}{B_0(\Psi)}, \quad 0$
$\Omega(\Psi)$	$\sqrt{\gamma\dfrac{P(\Psi)}{D(\Psi)}}\dfrac{M_{\varphi}(\Psi)-M_{\vartheta}(\Psi)}{R_0}, \quad \sqrt{\dfrac{P_{\parallel}(\Psi)}{D(\Psi)}}\dfrac{M_{\varphi}(\Psi)}{R_0}$
$H_{\mathrm{MHD}}(\Psi)$	$\gamma\dfrac{P(\Psi)}{D(\Psi)}\left(\dfrac{1}{\gamma-1}+M_{\vartheta}(\Psi)M_{\varphi}(\Psi)-\dfrac{1}{2}M_{\varphi}^2(\Psi)\right)$
$H_K(\Psi)$	$\dfrac{P_{\parallel}(\Psi)}{D(\Psi)}\left(\ln\left[\dfrac{\lvert D(\Psi)B_0(\Psi)-\Theta(\Psi)P_{\parallel}(\Psi)\rvert}{D(\Psi)B_0(\Psi)}\right]-\dfrac{1}{2}M_{\varphi}^2(\Psi)\right)$
$\Theta(\Psi)$	$\dfrac{P_{\perp}(\Psi)-P_{\parallel}(\Psi)}{P_{\perp}(\Psi)}\dfrac{D(\Psi)B_0(\Psi)}{P_{\parallel}(\Psi)}$
$T_{\parallel}(\Psi)$	$\dfrac{P_{\parallel}(\Psi)}{D(\Psi)}$
$S(\Psi)$	$\dfrac{P(\Psi)}{[D(\Psi)]^{\gamma}}$

Procedures (1)–(3) are repeated until convergence is reached, then the solution is interpolated onto the next (finer) grid. Unless otherwise specified, all numerical results presented in the following have been obtained with a grid of 256×256 points. Convergence is defined with a condition on the residual of equation (19). In each iteration Eq. (19) is solved using an over relaxation method with a red–black algorithm. Equation (19) is the only one requiring a boundary condition for its solution. For fixed boundary equilibria, we set $\Psi=$ constant on the boundary and determine the value of Ψ on the magnetic axis iteratively. Equation (15) does not pose any particular challenge, and can be solved by standard methods. Due to its algebraic nature, Eq. (16) can also be solved with a direct solver at each iteration. More precisely, a combination of the Newton–Raphson and bisection methods is used to accomplish the task.

The free functions representing the quasivariables of Table I are assigned as input parameters. If the MHD model is used, then the input free functions are

$$D(\Psi), \quad P(\Psi), \quad M_{\theta}(\Psi), \quad M_{\varphi}(\Psi), \quad B_0(\Psi),$$

representing a quasidensity, quasipressure, quasisonic poloidal Mach number, quasisonic toroidal Mach number, and quasitoroidal field, respectively. If the kinetic closure is used, the quasiparallel $(P_{\parallel}(\Psi))$ and perpendicular pressures $(P_{\perp}(\Psi))$ need to be assigned instead of the isotropic pressure $P(\Psi)$. Such free functions are intuitive and can be easily assigned as input to the code for describing standard tokamak equilibria. However, since the numerical solution is simplified by adopting the less intuitive functions $H(\Psi)$, $\Phi(\Psi)$, $\Omega(\Psi)$, $S(\Psi)$, $\Theta(\Psi)$, $T_{\parallel}(\Psi)$, $F(\Psi)$ in the implementation, the equations in Table II are used in the code for the conversion between free functions.

Notice that if the flow is purely toroidal [i.e., $\Phi(\Psi)=0$, $M_{\theta}(\Psi)=0$] the Bernoulli equation (16) is trivial, and

can be solved analytically at each iteration leading to the following explicit form of the density depending on the selected closure

$$\rho_K = D\frac{B}{B_0}\left|\frac{B_0-\Theta T_\parallel}{B-\Theta T_\parallel}\right| e^{[(R^2-R_0^2)\Omega^2]/2T_\parallel},$$
$$\rho_{\mathrm{MHD}} = D\left[1+\frac{1}{2}(R^2-R_0^2)\Omega^2\frac{\gamma-1}{\gamma}\frac{D}{P}\right]^{1/(\gamma-1)}. \tag{21}$$

As described earlier, if there is a poloidal component of the flow, then Eq. (16) needs to be solved numerically. In this paper, we focus our attention on relatively slow poloidal flows with a flow velocity smaller than the poloidal Alfvén velocity. Such flows are characterized by a poloidal Alfvén Mach number less than unity $M_{Ap}<1$ where $M_{Ap}=v_p\sqrt{\mu_0\rho}/B_p$ and B_p is the poloidal component of the magnetic field. Furthermore, poloidal flow is considered only within the MHD framework and the Bernoulli equation is Eq. (16) with $W=W_{\mathrm{MHD}}$. The roots of the Bernoulli equation yield the plasma density ρ which can be bracketed according to the following inequality:

$$\sqrt{\frac{B_p^2\Phi^2}{\mu_0(2H+R^2\Omega^2)}}<\rho<\left[\left(H+\frac{1}{2}R^2\Omega^2\right)\frac{\gamma-1}{\gamma S}\right]^{1/(\gamma-1)} \tag{22}$$

that can be easily derived from Eq. (16) and the definition of W_{MHD}. In the interval so defined, there can be either no sub-Alfvénic roots, 2 roots, or a single double root. In the first case, the poloidal flow is too fast, and must be reduced in order for sub-Alfvénic roots to exist. When two roots are found, the ''heavy'' root corresponds to subsonic flow, while the ''light'' root corresponds to supersonic flow with respect to the poloidal sound speed $C_{\mathrm{sp}}=C_sB_p/B$, where $C_s=\sqrt{\gamma p/\rho}$ is the sound speed. Clearly, the two roots become coincident if the considered point is on a transonic surface where the poloidal velocity varies from subsonic to supersonic. Since transonic equilibria are discontinuous,[7] the Bernoulli solver will need to perform the following tasks for each iteration:

(1) Identify the grid point where the 2 solutions of (16) are closest, and adjust the poloidal rotation velocity until they are closer than a specified tolerance.
(2) Make sure that (16) has solutions in all grid points, varying the poloidal flow until the condition is satisfied.

After identifying the point where the Bernoulli equation is degenerate (i.e., where the 2 solutions are coincident), the computational domain will be separated in two regions. In the inner region, the flow is assumed to be subsonic, so the ''heavy'' solution will be used. The outer region is assumed to have supersonic flow, so the ''light'' solution will be chosen. A similar type of equilibrium could be found with the opposite assumption (subsonic outer region and supersonic inner region), but this looks less interesting from the physical point of view, as the sound speed vanishes at the plasma edge and supersonic flow is more likely to develop near the plasma edge instead of the plasma core.

Some numerical difficulties in the code convergence may arise when dealing with large poloidal flows in high beta plasmas. Indeed, when the poloidal sonic Mach number $M_{\mathrm{sp}}=v_p/C_{\mathrm{sp}}$ is in the range

$$\frac{1}{1+\beta_\gamma}<M_{\mathrm{sp}}^2<\left(\frac{1}{1+\beta_\gamma}\right)\left[1+\frac{1}{4}\frac{\beta_\gamma}{(1+\beta_\gamma)^2}\frac{B_\theta^2}{B^2}\right], \tag{23}$$

then the Grad–Shafranov–Bernoulli system becomes hyperbolic and the elliptic solver used in FLOW may not converge. Here $\beta_\gamma=\mu_0\gamma p/B^2$ is assumed to be smaller than unity. Based on our past experience, we find that the numerical algorithm is convergent as long as the hyperbolic region is sufficiently small requiring that $\beta B_\theta^2/B^2\ll 1$ as indicated by (23). When the hyperbolic region is small and the algorithm is convergent, we expect the code results to be correct except inside the small hyperbolic region where the magnetic field could develop weak discontinuities proportional to β. This conclusion is based on a singular perturbation analysis of the equilibrium equation suggesting that the elliptic solution found with FLOW would provide the so-called outer and zeroth-order solution of the problem while the hyperbolic corrections would only appear in the higher β-order terms and be confined in the small hyperbolic region.

IV. FLOW RESULTS FOR EQUILIBRIA WITH PRESSURE ANISOTROPY AND TOROIDAL FLOW

In this section, we use the code FLOW to compute axisymmetric equilibria with pressure anisotropy and toroidal flow with applications to NSTX. The poloidal flow is neglected by setting $M_\theta(\Psi)=\Phi(\Psi)=0$. Because of its high betas, large fast-particle population and large toroidal velocities, the NSTX plasma is an ideal configuration to study these effects on the equilibrium. Because NSTX data analysis is typically carried out using available equilibrium and transport codes such as PEST (Ref. 25), EFIT (Ref. 26), and TRANSP (Ref. 27) which do not include toroidal rotation, it is likely that the code FLOW, described here, would benefit the NSTX work by retaining the effects of both pressure anisotropy and plasma rotation and could be used in combination with TRANSP to take into account the changes of the equilibrium induced by finite rotation.

A quantitative analysis is performed by numerically solving the equilibrium problem for an NSTX-like configuration including rotation and anisotropy. The free functions of Ψ used in the numerical study are power laws of the poloidal flux approximating realistic NSTX equilibria. The free function $D(\Psi)$ representing the density has been chosen to exhibit a rather flat profile while the parallel pressure is approximated with a fairly peaked function as shown below:

$$D(\Psi)\equiv D^E+(D^C-D^E)\left(\frac{\Psi}{\Psi_c}\right)^{0.1}, \tag{24}$$

$$P_\parallel(\Psi)\equiv P_\parallel^E+(P_\parallel^C-P_\parallel^E)\left(\frac{\Psi}{\Psi_c}\right)^3. \tag{25}$$

Here Ψ_c is the value of Ψ at the magnetic axis, and the superscripts E and C denote the values at the plasma boundary and magnetic axis, respectively. The pressure anisotropy

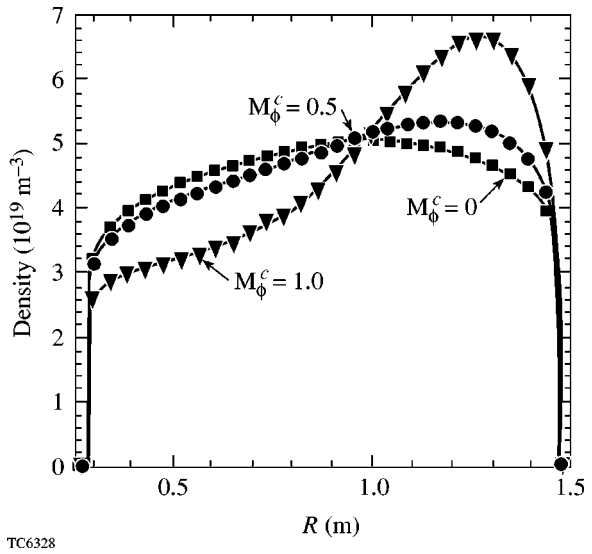

FIG. 1. Density shift for varying toroidal flow in an isotropic NSTX-like plasma.

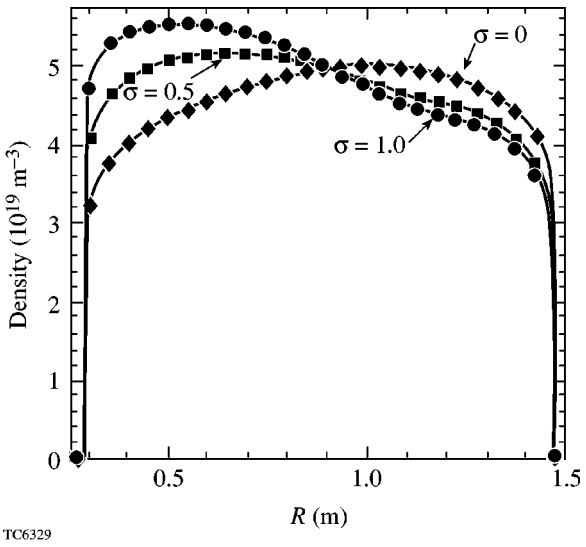

FIG. 2. Density profile shift in a static plasma for varying anisotropy for an NSTX-like equilibrium: $\sigma=0$ (diamonds), $\sigma=0.5$ (squares), $\sigma=1.0$ (circles).

is included by varying the constant factor σ in the definition of the free function $P_\perp(\Psi)$ describing the perpendicular pressure

$$P_\perp(\Psi)\equiv\frac{P_\parallel(\Psi)}{1+\sigma}. \tag{26}$$

When needed D^C and D^E are adjusted to keep the plasma mass constant. Similarly, $P_\parallel^E$ and $P_\parallel^C$ are also adjusted when the total energy needs to be conserved. We first focus our attention on the effects of rotation. Figure 1 shows a series of equilibria computed with the code FLOW assigning an increasing rotation as input for the code. The toroidal sonic Mach number is approximated with the following analytic function representing a velocity profile that is peaked in the center of the plasma column and nearly vanishes at the edge,

$$M_\varphi(\Psi)\equiv M_\varphi^c\left(\frac{\Psi}{\Psi_c}+0.01\right)^{0.2}, \tag{27}$$

where M_φ^c approximates the sonic Mach number at the magnetic axis. The flow velocity is varied by increasing the parameter M_φ^c from subsonic to supersonic values. When performing this analysis, some care must be used in the choice of the free functions of Ψ. In particular, since the plasma total mass is not an input variable, a control must be performed in order to make sure that the same amount of mass is contained in the plasma for all cases. A few iterations on the definitions of the free functions allowed to conserve the plasma mass within an error $\leqslant 2\%$.

The most dramatic consequences of an increasing rotation frequency is the growing shift of the density profile towards the outward region of the plasma column. In Fig. 1, the output of FLOW when M_φ^c is varied from 0 to 1 is shown. The picture consists of a line-cut along the midplane of the density profile, showing an increasing shift of the density peak with increasing rotation velocity. In particular, we observe that a relatively slow (subsonic) rotation does not produce a large variation of the profile. As the rotation increases, the plasma is squeezed against the outboard side of the boundary. Since the boundary itself is fixed, this will result in higher peaks and steeper gradients of the density profile in the outboard region of the plasma. The shift becomes large when the flow is about sonic. It is worthwhile to emphasize that the changes in the equilibrium profile produced by the presence of toroidal flow are only quantitative, and not qualitative. This also means that there is no dramatic change in the equilibrium properties as a purely toroidal flow goes from subsonic to supersonic. It should also be remembered that M_φ^c only approximately represents the maximum value of the sonic Mach number in the plasma, and that the actual Mach number will be more and more different from the free function of Ψ as the flow increases. Indeed, in the represented equilibrium with M_φ^c equal to 1, the actual maximum Mach number is about 1.5. This means that the equilibria shown in Fig. 1 do actually include both subsonic and supersonic flow equilibria.

Another interesting feature that can be analyzed with the code FLOW is the effect of pressure anisotropy on the equilibrium (see Fig. 2). As described in Ref. 6, the effect of anisotropy on the density profile is to increase the outward shift of the density if $\beta_\parallel<\beta_\perp$ and to decrease it if $\beta_\parallel>\beta_\perp$. This is qualitatively expressed by the following expression of the density shift:

$$\frac{d\rho}{\rho}=\left(1-\frac{\beta_\perp}{\beta_\parallel}\right)\frac{dB}{B}, \tag{28}$$

where d indicates a differential along the field lines, and $\beta_{\parallel,\perp}$ are parallel and perpendicular β.

As anisotropy is varied, some care needs again to be used in order to guarantee that the total energy of the plasma is kept constant for all cases. This is again performed with a few iterations on the definition of the free functions of Ψ, ensuring a variation of both total mass and energy $\leqslant 2\%$. The anisotropy is increased from an isotropic case ($P_\parallel(\Psi)=P_\perp(\Psi)$) to a case with $P_\parallel(\Psi)=2P_\perp(\Psi)$ and the param-

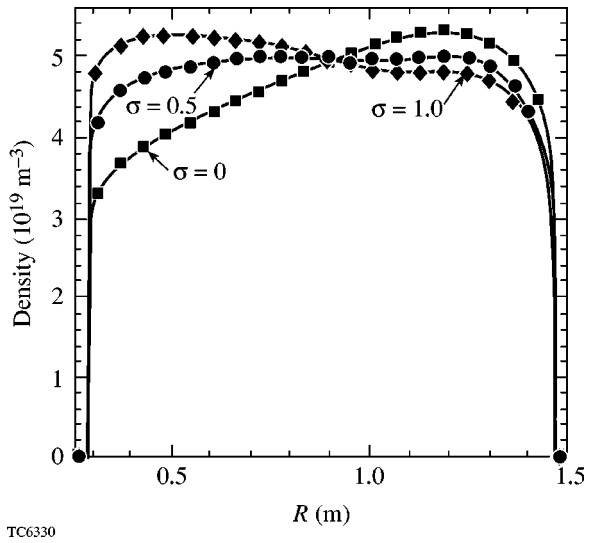

FIG. 3. Density shift in an NSTX-like plasma with toroidal flow for varying anisotropy: $\sigma=0$ (squares), $\sigma=0.5$ (circles), $\sigma=1.0$ (diamonds).

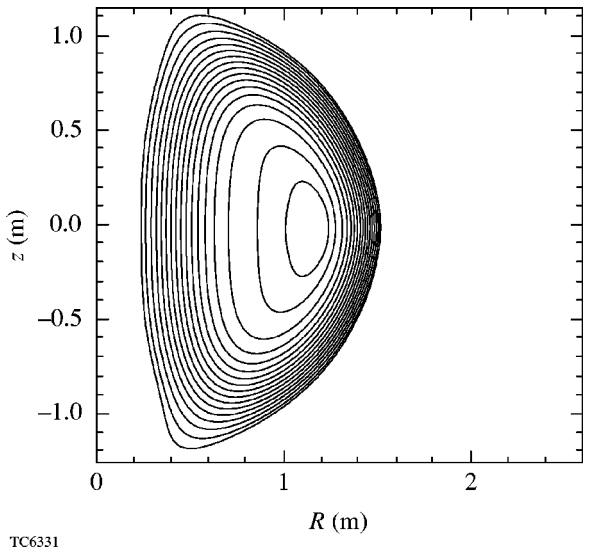

FIG. 4. Contour plot of magnetic surfaces in an NSTX equilibrium.

eter $\sigma\equiv((P_{\|}(\Psi)-P_{\perp}(\Psi))/P_{\|}(\Psi)$ has been used as a measure of the anisotropy. In obtaining the results shown in Fig. 2, the value of σ has been varied between 0 and 1, while no flow is introduced into the system. Details on the analytic expression of the free functions have been given in Eqs. (24)–(26). In agreement with the prediction of theory, an increasing value of σ produces an increasing inward shift of the density profile.

Comparing Figs. 1 and 2, it is apparent that strong anisotropy ($\sigma\sim0.5-1$) has an effect on the density profile of the same order of that of a moderate flow. In order to confirm this, we can compute equilibria where flow and anisotropy are present at the same time. We select the equilibrium with $M_{\varphi}^{c}=0.5$ shown in Fig. 1, and gradually increase the anisotropy, again varying σ from 0 to 1. In the same way as before, total energy and mass in the plasma are kept constant with an error $\leqslant2\%$. The resulting equilibria are shown in Fig. 3. Again, a line plot of density vs R is presented in the picture. It can be clearly seen that in this case an intermediate anisotropy ($\sigma=0.5$) completely balances the effect of toroidal rotation, while a larger anisotropy ($\sigma=1$) results in a net inward shift of the density profile.

The ability of the code to solve equilibrium problems with both macroscopic flow and pressure anisotropy suggests that FLOW can indeed be used to compute equilibria relevant to real experiments. Although this use is still in a preliminary phase, the result of such an equilibrium calculation, relative to the NSTX machine, is shown in Figs. 4–7. This equilibrium has aspect ratio ~1.5 and ellipticity ~1.9. Here all free functions of Ψ have been obtained from data provided by the NSTX team. In the considered equilibrium, toroidal flow and anisotropy are included, and the kinetic closure has therefore been used to compute this equilibrium.

Figure 4 shows the contour plot of the magnetic flux Ψ, while Fig. 5 shows the line plot of the magnetic flux Ψ vs the major radius of the plasma for two equilibria. The first one (labeled ''Flow'') has been computed with the input defined by the NSTX data, including toroidal rotation. The second one has been obtained with the same input for all free functions but the toroidal rotation, which has been set to 0. Figure 6 shows the line plot of the density for the two equilibria with and without rotation, indicating a significant flow-induced shift of the profile peak. Finally, Fig. 7 shows a line plot of the toroidal velocity along the midplane, with the peak velocity corresponding to a sonic Mach number of ~0.8. The plasma shape in this equilibrium is the same that has been used for the other equilibria in this same section, and constructed to closely reproduce the NSTX data.

V. EQUILIBRIUM WITH POLOIDAL FLOW

Because of the presence of profile discontinuities and hyperbolic regions, equilibria with poloidal flows are particularly challenging from the numerical point of view. Since poloidal flows are typically damped in tokamaks by the neoclassical poloidal viscosity, a steady flow needs to be driven.

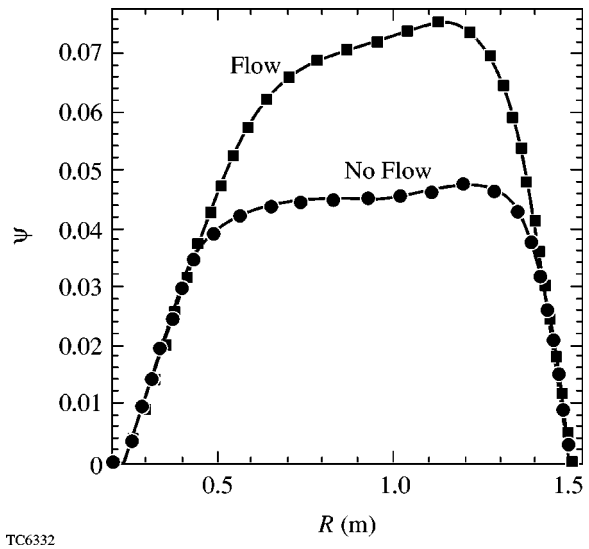

FIG. 5. Comparison of magnetic flux line plots along the midplane with and without flow in the same NSTX equilibrium.

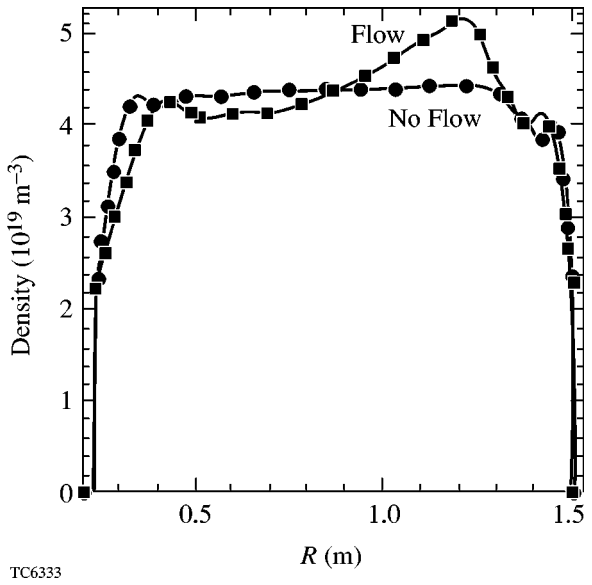

FIG. 6. Comparison of density line plots along the midplane with and without flow in the same NSTX equilibrium.

Different driving mechanisms have been proposed in recent years (see, e.g., Refs. 28–30) and detailed calculations of the neoclassical viscosity have been carried out in the different flow regimes (see Refs. 31 and 32). It is worth mentioning that neoclassical theories in the supersonic flow regimes have shown that the viscosity decreases as a power law of the Mach number $\nu_\theta \sim M_{\mathrm{sp}}^{-2}$ when the poloidal velocity exceeds the poloidal sound speed ($M_{\mathrm{sp}}>1$). This finding suggests that supersonic flows can be more easily driven than subsonic ones. Equilibria with a poloidal velocity below the poloidal sound speed are only weakly affected by the flow and therefore not particularly interesting for an in depth analysis of their equilibrium characteristics. Far more interesting are the moderately fast flows with a poloidal velocity profile ranging from subsonic to supersonic with respect to the poloidal sound speed. It is shown in Ref. 7 that such flows exhibit radial discontinuities in the pressure, velocity, and density profiles at the flux surface where the flow becomes transonic. The relative jumps in the equilibrium quantities scale as $\sim\sqrt{\epsilon}$, where $\epsilon = r_t/R_0$ is the inverse aspect ratio of the transonic surface. The origin of the discontinuous behavior at the transonic surface can be explained using the following simple gas dynamics considerations for a low-beta large aspect ratio torus with a circular cross section and a poloidal flow directed counterclockwise in the (R,z) plane.

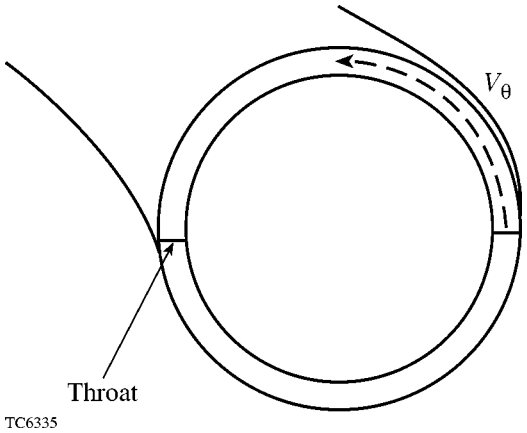

FIG. 8. Schematic representation of the magnetic deLaval nozzle.

In such a toroidal plasma, because of the frozen-in law, two adjacent flux surfaces can be thought of as the walls of a rigid "duct," with the cross section decreasing in the poloidal direction from the outer midplane ($\theta=0$) to the inner midplane ($\theta=\pm\pi$). In other words, the projection on the (R,z) plane of the streamlines coincides with the same projection of the flux surfaces. This situation is schematically represented in Fig. 8. The inboard side (labeled "throat") corresponds to the minimum cross section of the duct, while the outboard side corresponds to the maximum cross section.

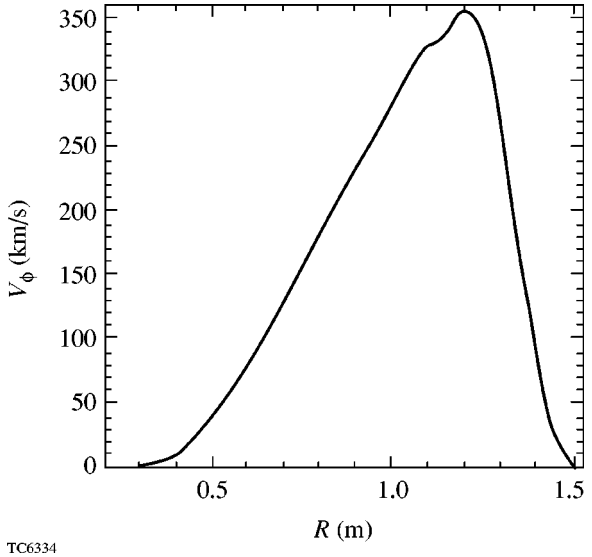

FIG. 7. Line plot along the midplane of toroidal velocity in an NSTX equilibrium.

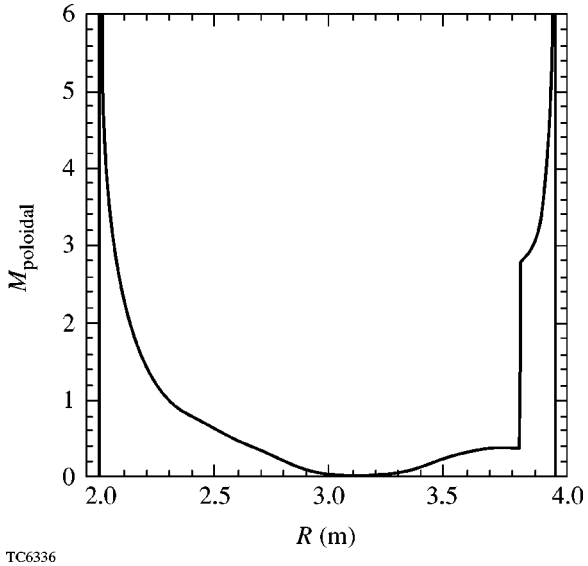

FIG. 9. Line plot of the poloidal sonic Mach number along the midplane showing the transonic discontinuity on the outboard side.

If the poloidal flow is subsonic at $\theta=0$ (with respect to the poloidal sound speed $C_{sp}=C_s B_p/B$), then it will accelerate along the duct, reaching the maximum velocity at the inner midplane. If the flow is sonic at $\theta=\pi$, it will be forced to become subsonic again after the throat, because of the periodicity constraint, and due to the fact that shock-induced discontinuities along the streamlines are not allowed at equilibrium.[7] Under the same token, if the flow is supersonic at $\theta=0$, then it will decelerate along the duct, possibly becoming sonic at $\theta=\pi$, but then it will be forced to accelerate again as the cross section increases. It follows that the flow can only be sonic on the inboard side $\theta=\pi$ and can only be either "well" subsonic or "well" supersonic on the outboard side ($\theta=0$). An interval of forbidden Mach number exists on the outboard side and a profile ranging from subsonic to supersonic will therefore develop a discontinuity on the outboard side as the flow must "jump" from well subsonic to well supersonic on a single flux surface.

The analysis in Ref. 7 shows that the solution of Eq. (16) for a low β, large aspect ratio tokamak can be written as

$$\frac{\rho(\theta,\Psi)}{D(\Psi)}\sim 1-\frac{1-M_\theta(\Psi)^2\pm\sqrt{(M_\theta(\Psi)^2-1)^2+2(\gamma+1)\epsilon\Lambda(\Psi)\cos\theta}}{\gamma+1}, \tag{29}$$

where $\Lambda=[1+(1-M_\varphi^2(\Psi))^2]$, and M_φ is the quasisonic toroidal Mach number. This solution is valid up to first order in $\epsilon^{1/2}$, where ϵ is the inverse aspect ratio at the transonic surface. In order to obtain sonic flow at a certain location, Eq. (29) must have two coincident solutions, i.e., the quantity under square root must vanish. Along a certain magnetic flux surface ($\Psi=$const.), the argument of the square root is however minimum for $\theta=\pi$. If the flow were sonic at any other angular location, Eq. (29) would clearly have no solution in all the region inboard of that point. This allows to conclude that the flow will be either sonic or supersonic at any angular location, but can be sonic only for $\theta=\pi$.

The outcome of the previous discussion is that a smooth transition between subsonic and supersonic flow is only possible at $\theta=\pi$, while everywhere else this can only occur with a radial discontinuity. More precisely, the discontinuity can be expressed analytically using Eq. (29) and leading to the following relative jump for the density:

$$\frac{[\rho]_{r_t^-}^{r_s^+}}{\rho}\simeq\sqrt{[\epsilon\Lambda]_{r_t}}\cos\frac{\theta}{2}, \tag{30}$$

where r_t is the transonic radius. Similar jump conditions are derived in Ref. 7 for the pressure, flow velocity, and Mach number.

Equilibria showing the properties herein described can be computed with FLOW for arbitrary aspect ratio and plasma shapes. An equilibrium of this kind, with circular cross section, is shown in Figs. 9–11. Such an equilibrium is computed starting from the following form of the free functions:

$$B_0(\Psi)=B_{0V}+(B_{0C}-B_{0V})\left(\frac{\Psi}{\Psi_C}\right)^3, \tag{31}$$

$$P(\Psi)=P_E+(P_C-P_E)\left(\frac{\Psi}{\Psi_C}\right), \tag{32}$$

$$D(\Psi)=D_E+(D_C-D_E)\sqrt{\frac{\Psi}{\Psi_C}}, \tag{33}$$

$$M_\theta(\Psi)=8M_\theta^{\max}\left[\frac{\Psi}{\Psi_C}-2\left(\frac{\Psi}{\Psi_C}\right)^2\right] \quad \text{if } \Psi\leqslant\Psi_t,$$

$$\frac{16}{9}M_\theta^{\max}\left(\frac{\Psi}{\Psi_C}+\frac{1}{2}\right)\left(1-\frac{\Psi}{\Psi_C}\right) \quad \text{if } \Psi\geqslant\Psi_t. \tag{34}$$

It is important to recognize that the free function for $M_\theta(\Psi)$ is chosen with a parabolic profile with an unspecified value $M_\theta^{\max}$ at the transonic surface. The location of the transonic surface is defined by the value of Ψ_t, which can be specified as a fraction of the maximum of Ψ occurring at the magnetic axis. Here, we have chosen $\Psi_t=0.25\Psi_{\mathrm{MAX}}$ to enforce that the transonic surface be located near the plasma edge characterized by $\Psi_{\mathrm{edge}}=0$. The value of the parameter $M_\theta^{\max}$ represents the maximum value of M_θ that guarantees the existence of real solutions for the Bernoulli equation. When $\Psi=\Psi_t$, $M_\theta=M_\theta^{\max}$ and there are two distinct solutions except for a single point on the transonic surface where the two solutions merge into one. Such a point is typically on

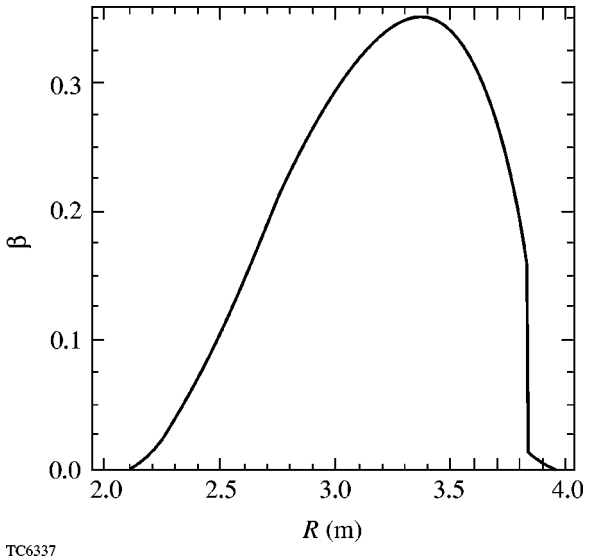

FIG. 10. Line plot of β along the midplane for a transonic equilibrium. The outboard jump occurs at the transonic surface.

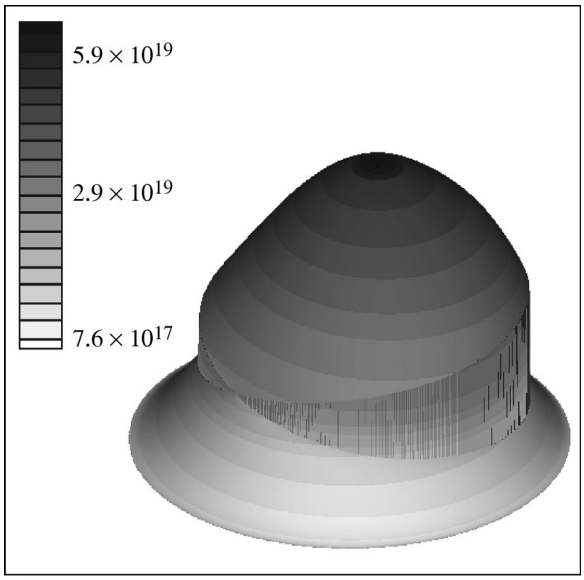

FIG. 11. 3D density plot for a transonic equilibrium showing the density jump at the transonic surface.

the inboard side at $\theta=\pi$ unless the plasma beta is sufficiently large to cause the ''throat'' to shift from the inboard to the outboard side. The value of $M_\theta^{\max}$ is not known *a priori*, and must be determined numerically by incrementally increasing $M_\theta^{\max}$ until a single root of the Bernoulli equation is found. Once Ψ_t and $M_\theta^{\max}$ are known, the plasma can be divided into an internal region with $\Psi>\Psi_t$ and external one with $\Psi<\Psi_t$. In both regions, the Bernoulli equation exhibits two distinct solutions corresponding to a subsonic and a supersonic root with respect to the poloidal sound speed. We have chosen the subsonic root in the internal region and the supersonic in the outer one. Obviously, the profile will exhibit a discontinuity at the transonic surface expect for the single point on $\Psi=\Psi_t$ where the two solutions merge.

Figures 9 and 10 contain line-cuts along the midplane of the poloidal Mach number ($M_{\rm sp}=V_p/C_{\rm sp}$) and of plasma beta for a tokamak equilibrium with major radius $R_0=3$ and minor radius $a=1$. Observe that both profiles are clearly discontinuous at the radius $R\sim 3.85$ corresponding to the outboard location of the sonic surface, i.e., the location where discontinuities are expected to be largest from the results of theory. As expected, the profiles are continuous on the inboard side, where the solution moves smoothly from the supersonic to the subsonic branch at the sonic surface (around $R\sim 2.3$). Figure 11 shows a three-dimensional plot of the density in $[\mathrm{m}^{-3}]$ emphasizing the modulation of the discontinuity along θ. The profile is continuous at $\theta=\pi$ and discontinuous elsewhere, with the size of the discontinuity increasing as one moves farther away from $\theta=\pi$.

The results presented in this section have been obtained by setting $M_\varphi(\Psi)=0$, resulting in the minimization of the toroidal flow. This will give, according to (30), the maximum size in discontinuities. In order to better resolve the discontinuities, we have also set the grid resolution to 512×512 points.

As a final comment on this paragraph, it is worthwhile to spend a few words on the numerical properties of the GS equation in this class of equilibria. As widely discussed in the literature, if the MHD approximation is used there is a narrow hyperbolic region for the GS equation close to the sonic surface, as described, e.g., in Ref 24. More precisely, assuming $\beta\ll 1$ and $B_\theta/B\ll 1$, it can be shown that the GS equation is hyperbolic in the range expressed by Eq. (23). Direct substitution of realistic values, such as those used for the equilibrium presented in Figs. 9–11, in Eq. (23) shows that the width of the hyperbolic region in term of $M_{\rm sp}^2$ is less than 0.1% and localized near the $M_\theta\simeq 1$ value. This implies that even though an elliptic solver is not appropriate to solve the GS equation in the hyperbolic region, the region of nonvalidity is so small that it does not affect the algorithm convergence and the final result is virtually independent of the hyperbolic region. Furthermore, the poloidal Mach number profile is discontinuous around the value $M_{\rm sp}=1$ in most of the domain, with the exception of the zone on the sonic surface around $\theta=\pi$. This implies that the hyperbolic region is removed from most of the computational domain and confined in a very narrow portion near $\theta=0$, $M_{\rm sp}\simeq 1$. As shown in Fig. 8, however, the poloidal Mach number profile is rather steep in its continuous section, and that will make the width of the hyperbolic region extremely narrow in the physical space. This argument is also strengthened by the fact that the plasma β is very small around the sonic surface, as shown in Fig. 10. To confirm the validity of this conclusion, a numerical study has been performed in order to identify the presence of a hyperbolic region in the equilibrium represented in Figs. 9–11. The result of such study is that even with the maximum resolution commonly used in the code (512×512 grid points), no hyperbolic region could be found.

VI. CONCLUSIONS

The effects of plasma flow on axisymmetric plasma equilibria have been analyzed using the code FLOW. The code solves the combined Grad–Shafranov–Bernoulli set of equations describing MHD equilibria with flow and finite pressure anisotropy. Purely toroidal flow is investigated in the context of NSTX-like equilibria where the effects of flow result in a significant outward shift of the plasma when the flow velocity is in the range of the sound speed. Other important alterations of the equilibrium profiles are caused by the finite pressure anisotropy causing an inward shift when $p_\parallel>p_\perp$ and an outward shift when $p_\perp>p_\parallel$.

The code FLOW is also used to investigate the effects of finite poloidal flow on tokamak equilibria. In particular, we confirm the analytic results of Ref. 7 indicating that radial discontinuities develop when the poloidal velocity profile varies from subsonic to supersonic with respect to the poloidal sound speed. FLOW shows that the solvability of the Bernoulli equation imposes a restriction on the admissible values of the poloidal Mach number at any poloidal location with the exception of $\theta=\pi$. Indeed, the flow profile can smoothly vary from subsonic to supersonic only in the inboard portion of the plasma column at $\theta=\pi$ while it requires a finite ''jump'' at any other poloidal location. The resulting equilibrium profiles of pressure, density, and velocity exhibit

a pedestal structure with a discontinuity at the transonic surface where the flow varies from ''well subsonic'' to ''well supersonic.''

ACKNOWLEDGMENTS

One of the authors (L.G.) would like to thank the Princeton Plasma Physics Laboratory Theory Department and the NSTX team for the assistance provided with the analysis of the NSTX equilibrium data. The authors would also like to thank Dr. Gardiner for assisting with the code development in its early stages.

This work has been supported by the U.S. Department of Energy under Contract No. DE-FG02-93ER54215.

[1]T. S. Taylor, H. St. John, A. D. Turnbull *et al.*, Plasma Phys. Controlled Fusion **36**, B229 (1994).
[2]T. S. Hahm and K. H. Burrel, Phys. Plasmas **2**, 1648 (1995).
[3]B. P. LeBlanc, R. E. Bell, S. Bernabei *et al.*, Phys. Rev. Lett. **82**, 331 (1999).
[4]M. Ono, S. M. Kaye, Y.-K. M. Peng *et al.*, Nucl. Fusion **40**, 557 (2000).
[5]R. J. Taylor, J.-L. Gauvreau, M. Gilmore, P.-A. Gourdain, D. J. LaFonteese, and L. W. Schmitz, Nucl. Fusion **42**, 46 (2002).
[6]R. Iacono, A. Bondeson, F. Troyon, and R. Gruber, Phys. Fluids B **2**, 1794 (1990).
[7]R. Betti and J. P. Freidberg, Phys. Plasmas **7**, 2439 (2000).
[8]F. L. Waelbroeck, Phys. Plasmas **3**, 1047 (1996).
[9]C. Wahlberg and A. Bondeson, Phys. Plasmas **7**, 923 (2000).
[10]J. P. Graves, R. J. Hastie, and K. I. Hopcraft, Plasma Phys. Controlled Fusion **42**, 1049 (2000).
[11]M. W. Kissick, J. N. Leboeuf, S. C. Cowley, and J. M. Dawson, Phys. Plasmas **8**, 174 (2001).
[12]R. Betti, Phys. Plasmas **5**, 3615 (1998).
[13]S. N. Bhattacharyya, Phys. Plasmas **1**, 614 (1994).
[14]R. L. Miller, F. L. Waelbroeck, A. B. Hassam, and R. E. Waltz, Phys. Plasmas **2**, 3676 (1995).
[15]D. J. Ward and A. Bondeson, Phys. Plasmas **2**, 1570 (1995).
[16]M. S. Chu, J. M. Greene, T. H. Jensen, R. L. Miller, A. Bondeson, R. W. Johnson, and M. E. Manuel, Phys. Plasmas **2**, 2236 (1995).
[17]R. Betti and J. P. Freidberg, Phys. Rev. Lett. **74**, 2949 (1995).
[18]R. Fitzpatrick and A. Aydemir, Nucl. Fusion **36**, 11 (1996).
[19]S. Chandrasekar, *Hydrodynamic and Hydromagnetic Stability* (Dover, New York, 1981), p. 481.
[20]S. Semenzato, R. Gruber, and H. P. Zehrfeld, Comput. Phys. Rep. **1**, 389 (1984).
[21]A. J. C. Beliën, M. A. Botchev, J. P. Goedbloed, B. van der Holst, and R. Keppens, J. Comput. Phys. **182**, 91 (2002).
[22]The JET Team, in *Plasma Physics and Controlled Nuclear Fusion Research 1992* (International Atomic Energy Agency, Wien, 1993), Vol. 1, p. 15.
[23]Y. Ishii, Y. Nakamura, and M. Wakatani, J. Plasma Fusion Res. **72**, 772 (1996).
[24]E. Hameiri, Phys. Fluids **26**, 230 (1983).
[25]R. C. Grimm, J. M. Greene, and J. L. Johnson, in *Methods in Computational Physics*, edited by J. Killeen (Academic, New York, 1976), Vol. 16, p. 253.
[26]L. L. Lao, H. St. John, R. D. H. Stambaugh, A. G. Kellman, and W. Pfeiffer, Nucl. Fusion **25**, 1611 (1985).
[27]R. J. Hawryluk, in *Proceedings of the Course in Physics of Plasmas Close to Thermonuclear Conditions*, Varenna, 1979 (CEC, Brussels, 1980), Vol. I, p. 19.
[28]A. B. Hassam, Comments Plasma Phys. Controlled Fusion **14**, 275 (1991).
[29]G. G. Graddock and P. H. Diamond, Phys. Rev. Lett. **67**, 1535 (1991).
[30]T. H. Jensen and A. W. Leonard, Phys. Fluids B **3**, 3422 (1991).
[31]K. C. Shaing, E. C. Crume Jr., and W. A. Houlberg, Phys. Fluids B **2**, 1492 (1990).
[32]A. B. Hassam, Nucl. Fusion **36**, 707 (1996).